Hot-Electron Preheat and Mitigation in Polar-Direct-Drive Experiments at the National Ignition Facility

A. A. Solodov,[1] M. J. Rosenberg,[1] M. Stoeckl,[1] A. R. Christopherson,[2] R. Betti,[1] P. B. Radha,[1] C. Stoeckl,[1] M. Hohenberger,[2] B. Bachmann,[2] R. Epstein,[1] R. K. Follett,[1] W. Seka,[1] J. F. Myatt,[3] P. Michel,[2] S. P. Regan,[1] J. P. Palastro,[1] D. H. Froula,[1] E. M. Campbell,[1] and V. N. Goncharov[1]

[1]Laboratory for Laser Energetics, University of Rochester
[2]Lawrence Livermore National Laboratory
[3]Department of Electrical and Computer Engineering, University of Alberta

The direct-drive approach to laser fusion is susceptible to hot-electron preheat due to the long-scale-length plasma conditions near the quarter-critical density of the target $n_c/4$ [where $n_c \approx 1.1 \times 10^{21}\,\lambda_0^{-2}\mathrm{cm}^{-3}$ is the critical density and λ_0 (in μm) is the laser wavelength]. This plasma is susceptible to parametric instabilities, such as stimulated Raman scattering (SRS),[1] that generate electrostatic plasma waves capable of accelerating electrons. For full-scale, direct-drive–ignition experiments, it is estimated that the target adiabat and performance will be negatively affected if more than ~0.15% of the laser energy is coupled into the cold fuel in the form of hot electrons.[2]

In this summary, we report measurements of hot-electron energy deposition in National Ignition Facility (NIF)–scale implosions. Surrogate ~2.4-mm-diam fuel capsules are driven in the polar-direct-drive (PDD) NIF geometry, which are only ~30% smaller than targets for the proposed ignition NIF PDD design.[3] We employ the multilayered target platform to study the hot-electron energy deposition profile in the imploding shell,[4] using mass-equivalent plastic targets with inner Ge-doped layers. Figure 1 shows (a) the laser power shape and [(b),(c)] targets with CH ablators and CH(Ge) payload. Different thicknesses of the Ge-doped layer (35 μm to 59 μm) were used, and the hard x-ray (HXR) emission was compared to the HXR emission from the reference all-CH target. The HXR emission was measured using the ten-channel NIF filter-fluorescer x-ray diagnostic.[5]

NIF target implosions were simulated using the 1-D hydrodynamic code *LILAC*.[6] *LILAC* simulations predict similar coronal conditions for all of the mass-equivalent targets, with a density scale length at the $n_c/4$ surface of 420 μm, an electron temperature of 3.5 keV, and an overlapped intensity of 4.5×10^{14} W/cm^2. Similar coronal conditions indicate similar laser–plasma interaction and hot-electron generation. Indeed, the measured SRS scattered-light spectra were almost identical in the experiments. The Monte Carlo code Geant4 (Ref. 7) modeled hot-electron transport, energy deposition, and bremsstrahlung emission in the imploding shell. Hot electrons were injected at the $n_c/4$ surface with a Maxwellian energy distribution and the temperature (T_{hot}), total energy, and divergence half-angle ($\theta_{1/2}$) were varied to best match the measured HXR spectra; $\theta_{1/2}$ was found to exceed 40° to 45°, the half-angle at which the dense shell is seen from the $n_c/4$ surface during the implosion.

Figure 1(d) shows the HXR spectra measured in the experiments and their best fits using the simulated spectra. The inferred hot-electron temperature is $T_{hot} = 56\pm2$ keV. The hot-electron energy deposition profile for the all-CH target, based on the simulation that best fits the data, is plotted in Fig. 1(e). It shows the cumulative hot-electron energy fraction in percent of the laser energy ($E_L = 720$ kJ) plotted as a function of the radial coordinate in the unimploded shell, measured from the inner shell radius. The inset shows the energy deposition in the unablated part of the shell in more detail. The red circles show the hot-electron energy deposition in the Ge-doped layers in the simulations of the multilayered targets plotted versus the mass-equivalent radius in the all-CH target. The inferred energy depositions in the multilayered and all-CH targets are in good agreement. Most of the hot-electron energy is deposited in the plasma that is ablated during the implosion. The energy deposited in the unablated shell ($R-R_{inner} < 79.5$ μm) is 0.4±0.05% of E_L, with only about half of this energy deposited in the inner 80% of the unablated shell.

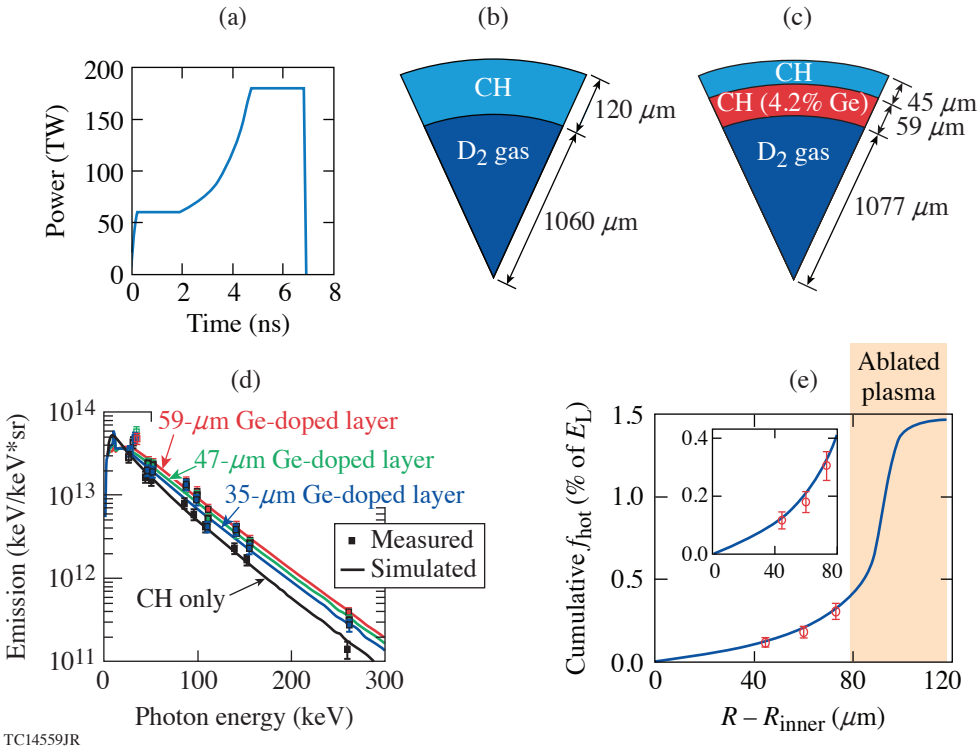

Figure 1
(a) The total laser power profile; [(b),(c)] design of targets with CH ablators; (d) measured and simulated time-integrated HXR spectra; (e) the cumulative hot-electron energy fraction for the all-CH target as function of the radial coordinate in the unimploded shell.

Thin layers of mid-Z material, such as Si, strategically placed in the ablator, can mitigate SRS and reduce hot-electron preheat. Figures 2(a) and 2(b) show the mass-equivalent targets having a buried Si layer in the ablator, designed to pass through the $n_c/4$ region during the laser flattop. This configuration shows significant reduction of SRS compared to the experiment without a Si layer. The inferred hot-electron temperature is $T_{hot} = 52 \pm 2$ keV. With a Si layer, hot-electron energy deposition in the unablated shell is reduced by about a factor of 2, demonstrating an important mitigation effect of the Si layer and providing a promising preheat-mitigation strategy that can expand the ignition-design space to higher intensities. Preheat extrapolation to ignition-scale cryogenic DT implosions on the NIF shows that by using a Si layer, preheat levels can be acceptable for on-target intensities close to 10^{15} W/cm^2.

This material is based upon work supported by the Department of Energy National Nuclear Security Administration under Award Number DE-NA0003856, the University of Rochester, and the New York State Energy Research and Development Authority.

1. W. Seka *et al.*, Phys. Fluids **27**, 2181 (1984); H. Figueroa *et al.*, Phys. Fluids **27**, 1887 (1984); C. S. Liu, M. N. Rosenbluth, and R. B. White, Phys. Fluids **17**, 1211 (1974).
2. J. A. Delettrez, T. J. B. Collins, and C. Ye, Phys. Plasmas **26**, 062705 (2019).
3. T. J. B. Collins *et al.*, Phys. Plasmas **19**, 056308 (2012); T. J. B. Collins and J. A. Marozas, Phys. Plasmas **25**, 072706 (2018).
4. A. R. Christopherson *et al.*, Phys. Rev. Lett. **127**, 055001 (2021).
5. M. Hohenberger *et al.*, Rev. Sci. Instrum. **85**, 11D501 (2014).
6. J. Delettrez *et al.*, Phys. Rev. A **36**, 3926 (1987).
7. S. Agostinelli *et al.*, Nucl. Instrum. Methods Phys. Res. A **506**, 250 (2003).

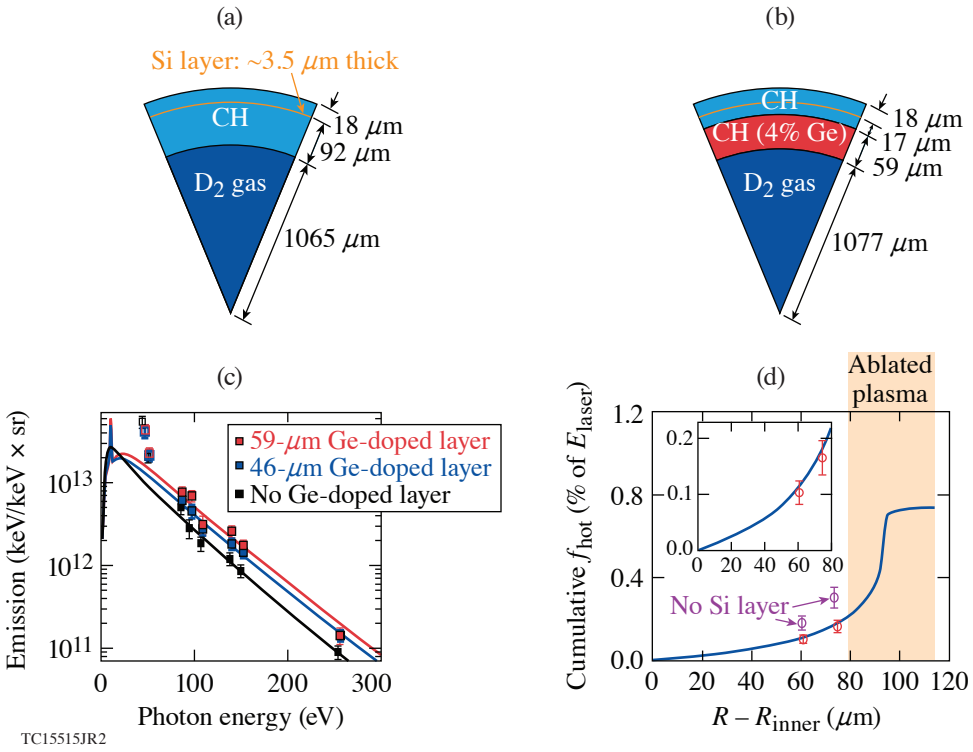

Figure 2
[(a),(b)] Targets with a Si layer in the ablator. (c) Measured and simulated time-integrated HXR spectra. (d) The cumulative hot-electron energy fraction for the target with a Si layer shown in (a) as a function of the radial coordinate in the unimploded shell.